EVOLUTION II -- FROM THE MAIN SEQUENCE THROUGH CORE HELIUM BURNING, $M = 3M_{\odot}$ *

ICKO IBEN, Jr.†

California Institute of Technology, Pasadena, California

UNPUBLISHED PRELIMINARY DATA

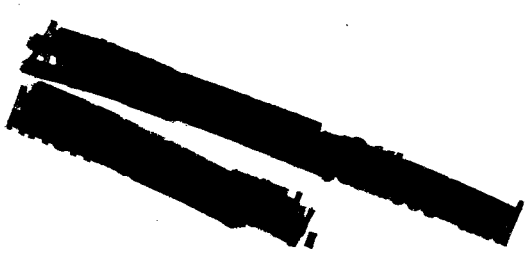

*Supported in part by the Office of Naval Research [Nonr-220(47)] and the National Aeronautics and Space Administration [NGR-05-002-028].

†Now at Massachusetts Institute of Technology.

ABSTRACT

A 3 $M_\odot$ stellar model of population I initial composition is evolved from the main sequence to the stage of helium exhaustion in the core. Out of the total time elapsed, three-fourths is spent near the main sequence with hydrogen burning in the core and one-fourth is spent in the red-giant region with helium burning in the core combined with hydrogen burning in a shell. During the hydrogen-burning phase near the main sequence, C^{12} is converted into N^{14} and Li is destroyed over a large fraction of the stellar interior. O^{16} is slowly converted into N^{14} in the core. During the rise toward the red-giant tip immediately preceding the ignition of helium in the core, the extension of a convective envelope almost to the hydrogen-burning shell then leads to an increase in the surface ratio of N^{14} to C^{12} by a factor of 3.2 and to a decrease in the surface abundance of Li by a factor of 60. Surface abundances do not change further during core helium burning. Comparison with the surface Li abundance of Capella F and G permits an inference concerning the average rate of mass loss from the surface of a 3 $M_\odot$ star.

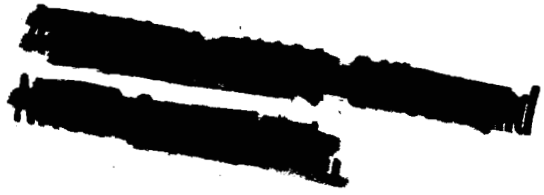

I. INTRODUCTION

The evolution of a 3 $M_\odot$ model of population I composition (X_H = 0.708, Z = 0.02) is followed through all phases beginning with core hydrogen burning near the main sequence and terminating in the red-giant region with the phase of helium exhaustion in the core.

The calculational procedures employed in constructing evolutionary models are described in paper I of this series (Iben 1965). The equation of state and opacity are the same as in paper I, with the exception that electron conduction opacity as used by Haselgrove and Hoyle (1956) is included.

During all phases, hydrogen burning reactions involving H^1, He^3, He^4, C^{12}, N^{14}, and O^{16} and helium-burning reactions involving He^4, C^{12}, N^{14}, and O^{18} are followed in detail. Hydrogen-burning reaction rates are the same as in paper I. Helium-burning reaction rates are given in section VI of this paper.

II. OVERALL FEATURES

One of the most gratifying fruits of evolutionary calculations is the establishment of a time-dependent relationship between the observable features and the interior characteristics of real stars.

The evolutionary path in the H-R diagram of the 3 $M_\odot$ model is shown in Figure 1. The times required by the model to reach circled points along the path are found in Table 1. Time is measured in units of 10^8 years from formation time as defined in paper I.

Relationships between observable features and events near the center of the star are shown in Figures 2 and 3. Using the format [Symbol = Description (Units)], dimensional variables in these figures are: L = luminosity

($L_\odot = 3.86 \times 10^{33}$ erg/sec), T_e = surface temperature (^oK), R = radius ($R_\odot = 6.96 \times 10^{10}$ cm), T_c = central temperature ($10^6\ ^oK$), and ρ_c = central density (gm/cm^3). In addition, M_{cc} = mass fraction in the convective core, L_{He}/L_H = rate of energy production by helium burning/rate of energy production by hydrogen burning, and X_i = abundance by mass of the i^{th} element (H^1, He^4, C^{12}, O^{16}, and O^{18}) at the stellar center. Time t is measured in units of 10^8 years from time of formation.

By comparing Figures 1, 2, and 3, one may correlate position in and rate of passage through a particular region of the H-R diagram with the dominant processes occurring in the interior and with the time scale associated with these processes.

The total time elapsed between formation and the phase of helium exhaustion in the core is approximately 3.26×10^8 yr. The main stage of hydrogen burning in the core (points 1 to 3 in Figure 1) lasts about 2.3×10^8 yr., or approximately three-fourths of the total time represented by the evolutionary calculations.

The phase of overall contraction immediately preceding the disappearance of the convective core (points 3 to 4) occupies roughly 10^7 yr. The extremely rapid core contraction and central temperature drop following the effective exhaustion of hydrogen near the center (points 4 to 4') occupies about 2.5×10^5 yr. The main phase of pure hydrogen shell-source burning (points 4' to 6) occupies about 10^7 yr. Rapid core contraction and rapid envelope expansion during pure hydrogen shell-source burning (points 6 to 10) carries the star to the beginning of red-giant evolution in about 4×10^6 yr.

Convection in the envelope of the star begins near point 10. Between points 10 and 13, the mass contained in the convective envelope is roughly proportional to log (L). Evolution toward the red-giant tip is halted

temporarily after approximately 9.0×10^5 yr at point 11 by ignition of the $N^{14}(\alpha,\gamma)F^{18}(\beta^+,\nu)O^{18}$ reactions in the core. To finally reach the tip of the red-giant branch (point 13), where the triple-α process begins in the core, requires another 3.34×10^6 yr.

Changes in the surface abundances of C^{12}, N^{14}, and Li occur in two stages lasting a total time of about 3×10^6 yr. The first stage terminates at point 11 where N^{14} α-burning in the core forces the star to descend to point 12. The second stage begins after the star reaches point 11 again at $t = 2.5160 \times 10^8$ yr and terminates at point 13 when $t = 2.5316 \times 10^8$ yr.

The main phase of core helium burning coupled with shell hydrogen burning (points 14 to 18) lasts for approximately 7.3×10^7 yr, or roughly one-fourth of the total evolutionary time represented. Out of a statistically large sampling of 3 $M_\odot$ stars, the number of stars burning helium and hydrogen in the red-giant region should therefore be approximately one-third of the number of stars burning only hydrogen near the main sequence.

III. HYDROGEN BURNING NEAR THE MAIN SEQUENCE

On reaching the main sequence, C^{12} has attained equilibrium with respect to N^{14} over that part of the interior which is involved in the production of He^4 during all subsequent phases. O^{16} has just begun to burn in the convective core.

The distribution within the star of temperature (T), density (ρ), pressure (P), luminosity (L), radius (R), and abundances by mass (X_i) of C^{12} (X_{12}), N^{14} (X_{14}), O^{16} (X_{16}), and He^3 (X_3) are given in Figure 4 as functions of mass fraction, just as the star reaches the main sequence (time $t = 2.4586 \times 10^6$ yr). Each variable in Figure 4 is scaled in such a way that the maximum value of

that variable in the stellar interior has the value unity.

From the distribution in luminosity and the distribution of C^{12} in Figure 4, it is evident that the reactions $C^{12}(p,\gamma)N^{13}(\beta^+ \nu)C^{13}(p,\gamma)N^{14}$ outside of the convective core contribute about 15 per cent of the total energy escaping the star.

Throughout the main hydrogen-burning phase, O^{16} in the convective core is converted slowly into N^{14} (points 1 to 3 in Figure 1, curve X_{16} in Figure 2). The increase in N^{14} prevents central density and temperature from rising as rapidly with time as would have been the case if the conversion of O^{16} to N^{14} had been neglected. In fact, during the first 7.5×10^7 yr, the product $X_1 X_{14}$ in the convective core increases from 3.93×10^{-3} to 6.3×10^{-3}, actually forcing central densities and temperatures to drop for a time in order to maintain equality between energy loss at the surface and energy production in the interior. At no time does O^{16} reach equilibrium with respect to N^{14}.

The convective core decreases in mass as the temperature at the core boundary increases and as the opacity at the core boundary -- due mainly to electron scattering -- decreases with decreasing numbers of electrons per gram. Luminosity rises, at first because of the increase in N^{14} ($t < 7.5 \times 10^7$ yr) and then because of the increase in average core temperatures and densities brought about by core contraction. Core contraction is necessary to maintain the pressure balance as the number of particles per gram in the core decreases.

During the first 6×10^7 yr of evolution off the main sequence, the region within which C^{12} is being reduced to equilibrium values with respect to N^{14} moves outward slowly to greater and greater mass fraction. At the same time, the envelope expands and cools to accommodate the increased energy flow from the interior. Eventually, the temperatures and densities in the $C^{12} \rightarrow N^{14}$

transition layer become too low for further conversion of C^{12} to N^{14} to take place. After 6×10^7 yr, the center of the transition layer (defined as the mass fraction at which C^{12} is reduced to one-half of its original value) is essentially fixed.

The distribution of state and composition variables within the star when hydrogen at the center has been reduced to approximately one-fourth of its initial value ($t = 1.9924 \times 10^8$ yr) is shown in Figure 5. The distribution of composition variables beyond mass fraction 0.25 is not altered further until the star approaches the red-giant region.

Note that the center of the transition region in which initial C^{12} has been considerably depleted is located at a mass fraction $(M_R/M_{STAR}) \sim 0.445$. The transition layer is not extremely sharp, but is reasonably symmetrical about the center. For order of magnitude estimates, one may therefore say that C^{12} has been depleted to equilibrium values in the inner 44.5 per cent of the star's mass.

The destruction of Li^6 and Li^7 has not been followed explicitly as a part of the evolutionary calculations. However, given the distribution of temperature and density versus mass fraction as it varies during evolution, it is a simple matter to calculate the reduction of Li at any given mass fraction. Adopting a center of mass cross-section factor of 100 keV barns for the $Li^7(p,\alpha)He^4$ reaction,

$$\frac{1}{X_7} \frac{dX_7}{dt} = 1.67 \times 10^7 \rho X_H \tau_{17}^2 e^{-\tau_{17}},$$

where X_7 denotes the abundance by mass of Li^7, $\tau_{17} = 84.53/T^{1/3}$, and T = temperature in 10^6 ^oK.

At a mass fraction of 0.985, temperature and density drop almost linearly

with time from 3.35×10^6 °K and 0.146 gm/cm^3, respectively, to 2.23×10^6 °K and 0.03 gm/cm^3 over a period of about 2.22×10^8 yr. At a mass fraction of 0.988, temperature and density drop from 3.11×10^6 °K and 0.112 gm/cm^3 to 2.05×10^6 °K and 0.024 gm/cm^3 over the same period.

A numerical integration reveals that, at mass fraction 0.985, Li^7 is reduced to about one-fourth of its initial value when $t \cong 2.24 \times 10^8$ yr. At a mass fraction of 0.988, Li^7 is reduced to about three-fourths of its initial value. Replacing the actual transition layer by a sharp discontinuity, one may say that Li^7 has been destroyed in the inner 98.66 per cent of the mass of the star by the end of the core hydrogen-burning stage.

Similarly, choosing the cross-section factor for the $Li^6(p,\alpha)He^3$ reaction as 2.5×10^3 keV barns, Li^6 is destroyed throughout approximately the inner 99 per cent of the star's mass.

During the main phase of hydrogen burning in the core, a balance between energy outflow and energy production is maintained by a gradual contraction and heating of the core. As core hydrogen abundance is reduced to lower and lower values, the rate of core contraction and heating is forced to increase until, when $t = 2.23669 \times 10^8$ yr (point 3 in Figure 1), continuity between the rapidly contracting core and an expanding envelope can no longer be maintained. The star suffers an overall contraction (points 3 to 4 in Figure 1) which lasts for a period of about 10^7 yr.

The variation of several central and surface characteristics toward the end of the period of overall contraction is shown on a slightly expanded scale in Figure 6. The quantity L_n represents the total rate of nuclear energy production in the star. The two curves M_{10} and M_{90} define the region within which 80 per cent of the nuclear energy is produced. Ten per cent of the total nuclear energy production occurs below mass fraction M_{10} and 10 per cent occurs

above mass fraction M_{90}.

Toward the end of the phase of overall contraction, the region of major nuclear energy production shifts away from the center as the temperature and density rise in the shrinking core is not sufficient to offset the decrease in core hydrogen abundance and as matter further and further from the center (in mass fraction) contracts to densities and temperatures sufficient to ignite hydrogen burning.

When $t \cong 2.507 \times 10^8$ yr, the decrease in the nuclear energy generation rate near the center overcomes the increase in the cross-sectional area through which energy flows. The consequent decrease in energy flux must be accompanied by a diminishing temperature gradient. Hence temperatures near the center drop at a rate which increases with proximity to the center. As a consequence of central cooling, fluxes near the center drop still more rapidly and the process of cooling during contraction is accelerated.

Hydrogen burning in the developing shell source is mildly explosive, causing matter slightly beyond the outer edge of the shell to expand. The region of expansion grows until it extends to the surface. Luminosity drops briefly (points 4 to 4' in Figure 1) as a consequence of absorption in the expanding envelope.

As matter in the hydrogen-depleted core becomes more nearly isothermal, the process of central cooling slows down. Semi-dynamic effects damp out quickly as the star adjusts to a balance between energy outflow and energy production almost entirely by non-explosive hydrogen burning in the new shell.

IV. THE MAJOR PHASE OF SHELL HYDROGEN BURNING

In about 10^5 yr following the disappearance of the convective core, hydrogen is effectively exhausted over the inner 6.6 per cent of the stellar mass. The major region of nuclear energy production now occurs in a fairly thick shell containing about 6 per cent of the stellar mass.

Throughout the entire period of increasing luminosity ($t = 2.34222 \times 10^8$ yr to $t = 2.44420 \times 10^8$ yr, points 4' to 6 in Figure 1), nuclear energy production in the shell increases as matter in the shell becomes slowly hotter, denser, and spatially closer to the center of the star. Just as during the stage of core hydrogen burning near the main sequence, the envelope of the star expands slowly to accommodate the increase in nuclear energy production. The mass contained in the shell decreases slowly as hydrogen is exhausted at the inner edge of the shell. Since contraction and heating persist for some distance beyond the region of nuclear energy production, the outer edge of the shell at first moves outward with time to larger mass fraction.

The distribution of state and composition variables within the star at a point approximately midway in the phase of increasing luminosity (point 5 in Figure 1, $t = 2.4012 \times 10^8$ yr) is shown in Figure 7. At this time, the region between the center and the base of the hydrogen-burning shell is nearly isothermal. Eighty per cent of the nuclear energy production occurs between mass fraction 0.080 and 0.124.

As the mass in the shell diminishes, the hydrogen content in the shell eventually decreases below a critical value (near point 6 in Figure 1, $t = 2.4486 \times 10^8$ yr). In an effort to maintain the high temperatures and densities in the narrowing shell, requisite for a balance between energy outflow at the surface and energy production in the shell, the hydrogen-exhausted core contracts and heats more rapidly. To keep in step with the receding core, the

center of mass of the shell moves more rapidly toward the center. As the shell moves inward to smaller radii, the flux of energy through the shell increases. The associated steepening of the temperature gradient through the shell is accomplished by expansion and cooling at the outer edge of the shell and heating at the contracting inner edge. The shell narrows rapidly in mass fraction as (1) hydrogen is depleted more rapidly at the inner edge of the shell where temperatures are rising and as (2) energy production decreases at the outer edge of the shell where temperatures are dropping.

The expansion initiated just outside the shell persists all the way to the surface of the star. With a decrease in temperatures and densities, the transmissibility of radiant energy through the expanding and cooling regions of the star decreases. The required decrease in luminosity is brought about at first by absorption in the expanding envelope and then by a decrease in the nuclear energy production rate in the narrowing shell.

It has been suggested (Hofmeister, Kippenhahn and Weigert 1964) that the rapid drop with time of the luminosity (between $t = 2.4486 \times 10^8$ yr, points 6 to 10 in Figure 1) is brought about entirely by an increase in the rate of absorption by the envelope. By comparing the variation of total luminosity, L, with the variation in the rate of nuclear energy production, L_n, (see curves log (L) and log (L_n) in Figure 6), it is evident that the ratio of envelope absorption to nuclear energy production increases less rapidly than the rate at which nuclear energy production decreases. The decrease in luminosity demanded by conditions in the expanding envelope is thus met primarily by a decrease in the rate of nuclear energy production.

The manner in which gas and composition characteristics change with time in the vicinity of the shell during the period of rapid core contraction coupled with rapid envelope expansion is shown in Figure 8. In addition to

quantities which have already been defined, matter velocity (v) is shown as a function of mass fraction. Subscripts 1 and 2 refer to the times $t_1 = 2.4786 \times 10^8$ yr and $t_2 = 2.4869 \times 10^8$ yr.

It may be seen that temperatures and densities over the major portion of the shell increase with time. At the very outer edge of the shell, temperatures and densities drop. From the curves v_1 and v_2 versus mass fraction, it is evident that matter at the leading edge of the shell is decelerated. The point at which contraction is replaced by expansion may be obtained from the relation $1/\rho\ (d\rho/dt) = \vec{\nabla} \cdot \vec{v} = 2v/R + (\partial v/\partial R)$. The neutral point ($d\rho/dt = 0$) occurs between the shell and the point at which velocity changes sign.

Even though temperatures and densities within the shell increase with time, they do not increase rapidly enough to offset the reduction in the total hydrogen content of the narrowing shell. As has already been noted, the net rate of nuclear energy production decreases with time.

Conditions throughout the star when it is near the end of the phase of decreasing luminosity are illustrated in Figure 9. Time $t = 2.4890 \times 10^8$ yr. From the distribution in luminosity one finds that the contracting core produces energy at the rate of $L_{core} \sim 7\ L_\odot$, the hydrogen-burning shell contributes $L_{shell} \sim 122\ L_\odot$, and the expanding envelope absorbs $L_{env} \sim 42\ L_\odot$. In the expanding envelope, the virial theorem holds true <u>locally</u> to a very good approximation. That is, one-half of the energy required to maintain local expansion is taken from local thermal energy and one-half is abstracted from the local energy flow. The situation in the envelope is thus just the reverse of the situation obtaining during contraction toward the main sequence as described in paper I.

The steep temperature gradient shown in Figure 9 between the center of the star and the shell has been built up during the phase of rapid core

contraction. It is a consequence of an increase in the gravitational energy production in the contracting core and of a decrease in the cross-sectional area through which energy flows through the radiative core. Since the temperature at the outer edge of the core is stabilized at a relatively constant value by the nuclear shell source, the necessary steepening of the temperature gradient is accomplished by a rise in core temperatures preferentially toward the center.

V. TO THE RED-GIANT TIP

When the minimum in luminosity is reached (point 10 in Figure 1, $t = 2.4893 \times 10^8$ yr) temperatures in the outer envelope have become so low that hydrogen and helium nuclei begin to combine with electrons over a considerable distance inward from the photosphere. As the stellar envelope continues to expand, the rising opacity and decreasing adiabatic gradient in the growing region of partial ionization lead to conditions more favorable for convection; convective energy transport supercedes radiative transport in a region which occupies more and more of the outer mass of the star.

On the other hand, the opacity in the shallow radiative region near the photosphere begins to drop as metals of low ionization potential become neutral and supply fewer electrons to form H^-. To maintain a sufficiently high level of flux through the surface, luminosity must rise.

The increase in luminosity is at first accomplished by a rearrangement of temperature and density in the growing convective region where changes in state variables are no longer explicitly restricted by the opacity. The convective region expands approximately adiabatically. That is, the energy required to expand a given layer in the convective region is supplied almost entirely by thermal energy from within this layer. Hence, as the mass in the radiative

region between the shell and the base of the convective region diminishes, the nuclear shell source is blanketed less strongly and delivers a larger fraction of its output to the surface.

The mass fraction beyond which energy is carried by convection is given by the curve M_{ce} in Figure 6.

The increasing surface demands cannot be met entirely by a decrease in the mass of the blanketing region of the star. Temperatures in the shell are therefore forced to rise fast enough to offset the decrease in shell hydrogen content, and nuclear energy production increases. (See curve log (L_n) in Figure 6, $t \geq 2.491 \times 10^8$ yr.) This illustrates forcefully that, contrary to the situation near the main sequence where hydrogen burning occurs over a relatively large mass fraction, nuclear energy production during shell hydrogen burning is highly sensitive to the properties of the stellar envelope.

The ignition of the $N^{14}(\alpha,\gamma)F^{18}$ reaction in the core when $t = 2.4982 \times 10^8$ yr (point 11 in Figure 1) temporarily stems core contraction and in fact (see the curve log (ρ_c) in Figure 6) leads to a slight central expansion. The central expansion in turn leads to a decreased rate at which temperatures rise in the shell. Shell energy production therefore diminishes. In order to adjust to the decreasing outward flow of energy, the stellar envelope must contract and the star moves downward in the H-R diagram (points 11 to 12 in Figure 1) along approximately the same path it followed upward. At the same time, the mass in the envelope through which energy flows by convection also decreases.

Prior to the growth of the convective envelope, the abundance of Li^7 in the outer 1.35 per cent of the star's mass remains constant and equal to its value near the main sequence. The Li^6 abundance remains constant over the outer one per cent of the star's mass. As the convective envelope extends inward beyond the original transition layers at which the Li abundances drop

sharply, unburned Li is convected inward until it is spread evenly over the entire convective region. The surface abundance of Li therefore drops.

At $t = 2.4866 \times 10^8$ yr, convection begins to extend into and beyond the original transition layer (mass fraction 0.455) separating the outer region, where C^{12} and N^{14} abundances have retained their main sequence values, from the inner region, where most of the original C^{12} has been converted into N^{14}. Thereafter, C^{12} is convected inward and N^{14} is convected outward. The surface ratio of N^{14} to C^{12} begins to increase.

At $t = 2.4980 \times 10^8$ yr, when its further extension is halted by N^{14} burning in the core, the convective envelope covers the outer 65.1 per cent of the star's mass. At this time, the surface abundance of Li^7 and Li^6 have been reduced relative to their main sequence values by factors of 48 and 65, respectively. The surface ratio of N^{14} to C^{12} has increased by a factor of 1.9.

As the star moves downward in the H-R diagram, the convective region decreases in mass and changes in surface abundances due to mixing are temporarily halted. When N^{14} near the center of the star has been reduced to nominal values (point 12 in Figure 1, $t = 2.5073 \times 10^8$ yr), core contraction and envelope expansion resume again. The star moves upward in the H-R diagram and the outer convective region again grows. When the mass fraction in the convective region exceeds 65.1 per cent (point 11 in Figure 1, $t = 2.5160 \times 10^8$ yr), surface abundances of Li, C^{12}, and N^{14} again begin to change.

At its maximum extent, when the star reaches the tip of the red giant phase of evolution (point 13 in Figure 1, $t = 2.5316 \times 10^8$ yr), the convective envelope covers the outer 82 per cent of the star's mass and reaches almost to the hydrogen-burning shell. The surface abundance of Li^7 and Li^6 have been reduced relative to their main sequence values by factors of 61 and 82, respectively. The surface ratio of N^{14} to C^{12} has been increased over the

main sequence ratio by a factor of 3.24.

The distribution of state and composition variables within the star at $t = 2.5315 \times 10^8$ yr (near point 13 in Figure 1) is shown in Figure 10. The triple-α process is just beginning to halt core contraction and the convective envelope has reached its maximum extent.

Note that the temperature at the base of the convective envelope (mass fraction 0.18) is only 1.24×10^6 °K. This is the maximum temperature which occurs in the outer convective region during the entire period of convective envelope growth. It is clear that neither Li nor C^{12} react with protons in the convective region and the changes in the abundances of these nuclei throughout the convective envelope are due entirely to mixing.

VI. THE MAJOR PHASE OF HELIUM BURNING IN THE CORE-1

Helium burning is limited to the reactions $3\ He^4 \rightleftharpoons C^{12*}(\gamma\gamma)C^{12}(\alpha,\gamma)O^{16}$ and $N^{14}(\alpha,\gamma)F^{18}(\beta^+\nu)O^{18}(\alpha,\gamma)Ne^{22}$. It is convenient to express reaction rates in terms of the quantities

$$r_{444} = (X_4)^3\ (\rho^2/T^3)\ \exp\ (52.7861-4317.35/T + S_o),$$

$$r_{412} = X_4\ X_{12}\ (\rho/T^2)\ \exp\ (86.1802-321.485/T^{1/3} - 8.9294/T^{2/3} + 1.5\ S_o),$$

$$r_{414} = X_4\ X_{14}\ (\rho/T^{3/2})\ \exp\ (51.6064-2866.72/T + 1.75\ S_o),$$

$$r_{418} = X_4\ X_{18}\ (\rho/T^{2/3})\ \exp\ (96.5207-400.502/T^{1/3} + 2\ S_o),$$

where ρ = density in gm/cm^3, T = temperature in 10^6 °K, X_i = abundance by mass of He^4, C^{12}, N^{14}, and O^{18}, and S_o is the weak screening factor defined in Appendix B of paper I. Reaction cross sections suggested by Fowler and Hoyle (1964) and by Caughlan and Fowler (1964) have been used.

The rate at which abundances by mass, X_i, of He^4, C^{12}, N^{14}, O^{18}, and Ne^{20} change with time via He^4-burning reactions may be written as

$$\frac{dX_4}{dt} = -3.97154\, M_H\, (r_{444} + r_{412} + r_{414} + r_{418}),$$

$$\frac{dX_{12}}{dt} = 11.9069\, M_H\, (r_{444}/3 - r_{412}),$$

$$\frac{dX_{14}}{dt} = -13.8944\, M_H\, r_{414},$$

$$\frac{dX_{16}}{dt} = 15.8708\, M_H\, r_{412},$$

$$\frac{dX_{18}}{dt} = 17.8595\, M_H\, (r_{414} - r_{418}),$$

$$\frac{dX_{22}}{dt} = 21.8207\, M_H\, r_{418},$$

where M_H = mass of the hydrogen atom in gm.

The contribution of helium burning reactions to the energy generation rate is

$$\epsilon_\alpha = \Sigma\, r_{ij}\, \epsilon_{ij}$$

$$= (0.388767\, r_{444} + 1.14515\, r_{412} + 1.05688\, r_{414} + 1.54743\, r_{418}) \times 10^{-5} \text{ erg gm}^{-1} \text{ sec}^{-1}.$$

The temporary core expansion and envelope contraction initiated by the $N^{14}(\alpha,\gamma)F^{18}(\beta^+\nu)O^{18}$ reactions have been described in section V. Core contraction is again halted when central temperatures and densities reach sufficiently high values to fire the triple-α process. Initially, a major fraction of the energy produced by helium burning is used up in supporting core expansion.

However, within about 10^6 yr after the ignition of the triple-α process, semi-dynamic changes are damped out in the sense that the rate at which energy is transferred to and from the gravitational field becomes negligible everywhere relative to the rate of energy production by nuclear sources.

Over a period of about 4×10^7 yr, the total rate of nuclear energy production drops as the rise in shell temperatures and densities is inhibited by core expansion. The decrease in nuclear energy production forces the stellar envelope to contract. This contraction in turn helps to maintain high enough temperatures and densities in the hydrogen-burning shell to permit a balance between energy outflow and energy production.

The high density and temperature dependence of the triple-α process leads to the formation of a convective core which, after an initial overshoot, grows slowly with time until core helium burning is almost completed. The high density and temperature dependence is also responsible for the fact that central densities continue to drop as central temperatures rise, long after the semi-dynamic effects associated with the ignition of a new fuel have been damped out.

When $t \cong 2.7625 \times 10^8$ yr, the mass in the convective envelope has been reduced sufficiently that changes in envelope opacity begin to influence the rate of nuclear energy generation in the shell. The luminosity begins to rise. Conditions within the star when it is near the relative minimum in luminosity ($t = 2.7579 \times 10^8$ yr) are shown in Figure 11. Note that the helium-burning core produces only about one-eighth as much energy per second as the hydrogen-burning shell. The conversion of N^{14} to O^{18} occurs in a thin shell between the convective core and the hydrogen shell source; this conversion provides a negligible contribution to the total luminosity.

As C^{12} is built up by the triple-α process, energy production by the $C^{12}(\alpha,\gamma)O^{16}$ reaction becomes more important. At $t \cong 3.006 \times 10^8$ yr, C^{12}

reaches equilibrium with respect to creating and depleting reactions and energy production by the $C^{12}(\alpha,\gamma)O^{16}$ reaction begins to dominate over energy production by the triple-α source. Conditions within the star when $t = 2.9920 \times 10^8$ yr are shown in Figure 12. The major source of energy escaping the star is still the hydrogen-burning shell. Helium-burning reactions in the core contribute only one-sixth as much energy as the hydrogen-burning reactions in the shell.

As the $C^{12}(\alpha,\gamma)O^{16}$ reaction becomes increasingly dominant over the triple-α source, central densities drop less rapidly until, when $t = 3.119 \times 10^8$ yr, central densities begin to rise. This is partially a result of the decreasing density dependence of the effective core source and partially a result of the decrease in the number of particles per gram in the core.

Between $t \cong 3.08 \times 10^8$ yr and $t \cong 3.20 \times 10^8$ yr, the relation between observable variables and core structure is very similar to that obtaining during core hydrogen burning near the main sequence. Stellar radius and luminosity increase as central temperature and core energy production rise.

When $t \sim 3.2 \times 10^8$ yr, however, the sensitivity of the shell energy production rate to small changes in structure is again manifested. As the helium abundance in the core drops, the core is forced to contract and heat more rapidly. Just or during the period of rapid core contraction and envelope expansion described in section IV, the luminosity decreases as the envelope absorbs energy and the shell source decreases in strength.

The period of core helium exhaustion begins when $t \cong 3.25 \times 10^8$ yr. Structural variations are thereafter very similar to those during and following the core hydrogen exhaustion phase described in sections III and IV. The decrease in the rate of nuclear energy production near the center causes the convective core to diminish rapidly and leads to a drop in central temperatures.

Luminosity rises as matter in a newly developing helium-burning shell contracts to higher densities and temperatures.

Conditions within the star when $t = 3.2633 \times 10^8$ yr are shown in Figure 13. Nuclear energy production now occurs predominantly in two shells -- a helium-burning shell which is growing in strength, and the hydrogen-burning shell which is diminishing in strength. A third shell in which N^{14} is being transformed into O^{18} is also evident.

As is well known, the cross section for the $C^{12}(\alpha,\gamma)O^{16}$ reaction under stellar conditions is uncertain by at least a factor of ten. The reaction rate adopted in this paper is near the maximum allowed theoretically and, as may be seen from the curves X_{16} vs t and X_{12} vs t in Figure 2, leads to a nearly pure O^{16} core at the end of core helium burning. A simple calculation shows that a reduction in the $C^{12}(\alpha,\gamma)O^{16}$ rate by a factor of ten would lead to final C^{12} and O^{16} abundances in the core of about $X_{12} \sim 0.65$, $X_{16} \sim 0.33$.

The uncertainty in the $C^{12}(\alpha,\gamma)O^{16}$ reaction rate will have an extremely important effect on the evolutionary behavior of the star following the phase of core helium exhaustion. Fortunately, however, the variation of observable characteristics with time during the main phase of core helium burning is not particularly sensitive to the effective reaction rate chosen for the $C^{12}(\alpha,\gamma)O^{16}$ reaction. This is because energy production in the hydrogen-burning shell strongly dominates energy production in the helium-burning core (see the curve L_{He}/L_H in Figure 3). The major effect of the core source is simply to prevent rapid core contraction, causing the change in observable characteristics to proceed on a nuclear burning time scale rather than on a gravitational time scale.

It should be finally remarked that O^{18} begins to react with alpha particles at the same time that the triple-α process begins in the core.

By the end of the major core helium-burning phase, O^{18} in the core has been converted entirely into Ne^{22}. It has been suggested (e.g., Clayton 1964) that the $Ne^{22}(\alpha,n)Mg^{25}$ reaction might be a source of neutrons for the synthesis of s-process elements. Very little applicable experimental data exists for this reaction, however a fairly generous upper limit to the cross section may be obtained by assuming that there are numerous resonances above and below the 481.6 keV threshold. Even with this upper limit, no significant conversion of Ne^{22} into Mg^{25} occurs at the temperatures and densities encountered by the 3 $M_\odot$ model star as far as it has been evolved. It is expected that central temperatures in the 3 $M_\odot$ model will continue to drop below the maximum of $T_c = 1.6 \times 10^8$ °K encountered, until He^4 is completely exhausted in the core. Furthermore, the temperatures and densities in the helium-burning shell will be very close to those obtaining in the core during core helium burning. It is concluded that the $Ne^{22}(\alpha,n)Mg^{25}$ reaction will not serve as a neutron source for s-process synthesis in helium-burning regions of a 3 $M_\odot$ star during quasistatic stages of evolution. This conclusion is subject to the proviso that neutrino losses (by the photoneutrino process and pair annihilation) from the helium-exhausted core will not significantly affect the average temperature and density in the helium-burning shell.

VII. OBSERVATIONAL TESTS

A. The Li Content of the F and G Components of α-Aurigae

Wallerstein (1965) has recently observed in two components of α-Aurigae a difference in surface Li abundance amounting to a factor larger than 100. The less luminous "F" component ($M_v \sim 0.37$, $M \sim 2.9\ M_\odot$, spectral type F8, $\log T_e \sim 3.72 \rightarrow 3.76$) has a surface Li abundance about 100 times larger than the solar value. The Li abundance in the more luminous "G" component

($M_V \sim 0.12$, $M \sim 3.0\ M_\odot$, spectral type G5, $\log T_e \sim 3.67 \rightarrow 3.70$) is below the limit of detectability.

Assuming that both components are of the same age and of the same initial composition, the more massive G component has presumably evolved further than the less massive F component. The two components are close enough in mass and the mass determinations are themselves sufficiently uncertain that a preliminary discussion centered about a single model of 3 $M_\odot$ is permissible. The cross-hatched portions in the H-R diagram of Figure 1 indicate roughly the regions in which the model equivalents of the F and G components of Capella probably lie.

It is clear that the less evolved F component has not quite reached the stage at which convection begins to alter the surface Li content, whereas the G component has already completed the stage of surface abundance changes and has embarked on the relatively long period of core helium burning coupled with hydrogen shell-source burning.

The fact that the observed depletion of surface Li is larger, by at least a factor of 1.7, than that obtained with the models may be ascribed to several effects which have been neglected in the calculations.

(1) Models have been constructed with very crude opacities. With better opacities, the rearrangement of interior temperatures and densities might lead to a destruction of Li^7 over the inner 99.2 per cent of the star's mass during evolution near the main sequence rather than over the 98.65 per cent discussed in section III. During the passage to the red giant tip, surface Li^7 would be reduced by the factor of 100 required for consistency with the observations.

It is more likely, however, that the increased opacity expected when line absorption is included will lead to lower temperatures and densities in the

outer portions of the star during evolution near the main sequence. More accurate opacities will therefore probably decrease the predicted alteration in surface Li content and the key to the discrepancy must be found elsewhere.

(2) The mass of the G component may be somewhat larger than 3 $M_\odot$. As model mass is increased, envelope temperatures at corresponding stages of evolution near the main sequence also rise. Hence, for a more massive star, the interior mass fraction over which Li is destroyed during core hydrogen burning is larger and the decrease in surface Li content on reaching the red giant tip is correspondingly greater.

(3) The most probable explanation of the existing discrepancy is surface mass loss during or prior to the growth of the convective envelope. Mass loss will reduce the total amount of unburned Li remaining near the surface of the star. As convection extends beyond the lower boundary of the layer of unburned Li, the reduction in the surface Li abundance brought about by mixing will proceed more rapidly and to lower final values of surface Li than would have been the case if no mass loss had occurred.

Since the surface Li abundance in Capella F is so high, it is reasonable to suppose that this abundance has undergone no change during the entire period of evolution from the main sequence. In order not to have bared its Li-depleted interior, Capella F must have lost less than 0.04 $M_\odot$ of its original main sequence mass. An upper limit to the average rate of mass loss over the 2.5×10^8 yr elapsing between reaching the main sequence and reaching the stage of convective envelope growth is therefore about 1.6×10^{-10} $M_\odot$/yr.

However, during the passage from the main sequence to the vicinity of Capella F, the total Li^7 content of the star need be reduced by only 40 per cent (over that found by calculations without mass loss) in order to lead eventually to a reduction in surface Li^7 abundance at the red giant tip by

a factor of 100. Hence, a more modest average mass loss rate of $\sim 6 \times 10^{-11}$ $M_\odot$/yr leads to consistency with the observations. A similar argument holds for Li^6 which, in any case, is expected to be much less abundant than Li^7.

If the mechanism driving surface mass loss is correlated with the extent of turbulent activity in sub-photospheric layers, one might expect a sharp increase in the rate of mass loss just as the convective envelope in the star begins to grow inward. Assuming that Capella F and G are of the same age and that Capella G has experienced mass loss at a constant rate in passing from the onset of envelope convection to its present position in the H-R diagram, it is possible to obtain a rough estimate of the mass loss rate while energy is carried by convection in the stellar envelope.

To obtain this estimate, it is necessary to interpolate from evolutionary models of different mass (see, e.g., Iben 1964). One finds that times t_c of about 5.5×10^8 yr, 2.49×10^8 yr, 7.0×10^7 yr, and 2.2×10^7 yr are required by models of mass $(M/M_\odot) = 2.25$, 3.0, 5.0, and 9.0, respectively, to evolve from formation to the start of envelope convection during shell hydrogen burning. In the neighborhood of 3 $M_\odot$, an additional time amounting to about 16 per cent of t_c is required to pass from the start of envelope convection to the vicinity of Capella G.

By interpolation one finds that Capella F ($M \sim 2.9$ $M_\odot$) has required about 2.69×10^8 yr to reach its present position. Neglecting the time required to pass from the vicinity of Capella F to the onset of envelope convection, one may conclude that Capella G reached the start of envelope convection at a time $t_c \sim 2.69 \times 10^8$ yr/1.16 = 2.32×10^8 yr. Again by interpolation one finds that Capella G must have had an initial mass close to 3.08 $M_\odot$. The inferred mass loss rate during the period of envelope convection is thus $(3.08\ M_\odot - 3.0\ M_\odot)/3.7 \times 10^7$ yr = 2.2×10^{-9} $M_\odot$/yr.

A mass loss rate even of this magnitude will have little effect in reducing the total Li content during the period of convective envelope growth. For only about 10^5 yr are required for convection to cover the outer few per cent of the star's mass. And once convection extends beyond the base of the original layer of unburned Li, mass loss from the increasingly Li-impoverished surface becomes less and less effective in reducing the total Li content of the star.

In summary, the difference in the surface Li abundances of Capella F and G can be accounted for in a very natural way as a result of (a) a reduction in the total Li content by nuclear burning in the interior and mass loss at the surface followed by (b) a reduction in the surface Li abundance by a mixing of the remaining unburned Li over most of the stellar interior during the passage to the red giant tip.

B. The Surface Ratio of N^{14} to C^{12}

Because of the much greater mass fraction within which C^{12} has not been burned, the change in the surface ratio of N^{14} to C^{12} will be very little affected by the mild mass loss inferred in the preceding paragraphs. A determination of the N^{14}/C^{12} ratio in Capella F and G would therefore provide a clearer test of convective envelope extention and at the same time provide direct evidence for the occurrence of the reaction $C^{12}(p,\gamma)N^{13}(\beta^+\nu)C^{13}(p,\gamma)N^{14}$ at rates suggested by nuclear astrophysicists. At the surface temperatures assigned to Capella F and G, an analysis of molecular lines of CO, CN, and NO may be marginally possible. The surface ratio of total N^{14} to total C^{12} in Capella G should be 3.24 times larger than that in Capella F if, in Capella F, the ratio by mass, $(X_{14}/X_{12})_F$, is 1/3. A simple extension of the results obtained in previous sections leads to the general relationship

$$(X_{14}/X_{12})_G \cong 3/2\ (X_{14}/X_{12})_F + 7/12.$$

For a number of reasons, an interpretation of the observational results cannot be entirely unambiguous. For example, all other things being equal, if the $C^{12}(p,\gamma)N^{13}$ center of mass cross section factor has been overestimated, then the interior mass fraction over which C^{12} has been converted into N^{14} has also been overestimated; the ratio of N^{14} to C^{12} at the red giant tip should be smaller than that found here. However, the extent of mixing and reduction of surface abundances is also influenced by the penetration of convection beyond the formal boundary between the regions of stability and instability against convection. The additional increase in the final surface N^{14}/C^{12} ratio due to penetration might well mask the error introduced by a faulty estimate of the $C^{12}(p,\gamma)N^{13}$ reaction rate. Since the point at which evolution vertically upward toward the red giant tip is finally halted depends on the effective density and temperature at which the triple-α process becomes important, the maximum depth to which convection extends at the red giant tip is influenced by the intrinsic rate of this process. If the cross section for the $Be^{8*}(\alpha,\gamma)C^{12}$ reaction is actually larger than that assumed here, then the maximum depth of the formal convective-radiative boundary has been overestimated; the increase in the N^{14}/C^{12} surface ratio has consequently also been overestimated.

Finally, there are the uncertainties associated with the use of crude opacities, a crude equation of state, crude nuclear screening parameters, etc. The assessment of such uncertainties is best accomplished by further model construction with improved constitutive relations.

C. An Inference Concerning the Role of the $N^{14}(\alpha,\gamma)F^{18}$ Reaction in Low Mass Stars

In 3 $M_\odot$ evolution, the $N^{14}(\alpha,\gamma)F^{18}(\beta^+\nu)O^{18}$ reactions stop core contraction briefly at a luminosity considerably lower than that at which the triple-α process terminates the rise along the nearly vertical red giant branch. In less massive stars, electrons in the hydrogen exhausted core will be quite degenerate when central temperatures become high enough to fire the $N^{14}(\alpha,\gamma)F^{18}$ reaction. Under conditions of electron degeneracy, most of the nuclear energy liberated remains in the core, raising core temperatures rapidly until degeneracy is lifted.

The nuclear content of the hydrogen-exhausted core is primarily alpha particles and there are two electrons for every alpha particle. At an abundance by mass of 0.01, N^{14} can liberate approximately 5 keV per dominant particle. This is enough energy to raise core temperatures by 75 million degrees, quite sufficient to ignite the triple-α process. Progress vertically upward along the red giant branch will thus be finally, not temporarily, halted when the $N^{14}(\alpha,\gamma)F^{18}$ reaction is fired in the degenerate core of a light population I star.

In a light population II star, however, the small amount of N^{14} in the core will be too small to raise temperatures to the triple-α ignition point. After the exhaustion of N^{14}, the core will remain electron-degenerate and the upward rise along the red giant branch will continue until core temperatures, rising solely because of gravitational contraction, reach the triple-α ignition point.

In two clusters composed of similar-mass stars, the tip of the red giant branch should be higher in that cluster having the lower initial (surface)

heavy element content. A comparison of the old population I cluster NGC188 with any population II cluster, e.g., M92, suggests that this explanation has some merit.

ACKNOWLEDGMENTS

The author would like to express thanks to William A. Fowler for making available funds from the Office of Naval Research and the National Aeronautics and Space Administration; G. D. McCann for providing time on the Cal Tech IBM 7094 when funds were exhausted; and Ken Hebert and Steve Caine for programming assistance above and beyond the call of duty. He is deeply indebted to William A. Fowler for granting the freedom to pursue research on ordinary stars and to members of the Physics and Astronomy Departments and of the Kellogg Radiation Laboratory at Cal Tech for providing an environment conducive to this research. He is indebted to the Physics Department at MIT for its hospitality during the writing of this paper and to the MIT Graphic Arts facility for its excellent work.

TABLE 1

EVOLUTIONARY LIFETIMES

point	1	2	3	4	4'
time	0.024586	1.38921	2.23669	2.34089	2.34222
point	5	6	7	8	9
time	2.40119	2.44420	2.47004	2.47865	2.48429
point	10	11	12	13	14
time	2.48925	2.49817	2.50728	2.53163	2.55850
point	15	16	17	18	19
time	2.78126	2.94233	3.06968	3.19043	3.23566
point	20				
time	3.26323				

TABLE 2

MAXIMUM VALUES OF INTERIOR PARAMETERS

Figure	Time*	P_c †	T_c ‡	ρ_c §	L‖	R #	X_H (H^1)	X_3 (He^3)	X_4 (He^4)	X_{12} (C^{12})	X_{14} (N^{14})	X_{16} (O^{16})	X_{18} (O^{18})	X_{22} (Ne^{22})
4	0.02459	1.350	24.08	41.33	94.95	1.396	0.7080	2.517×10^{-5}	0.2734	3.610×10^{-3}	5.484×10^{-3}	1.080×10^{-2}		
5	1.9924	0.9996	26.31	46.36	129.1	2.125	0.7080	3.609×10^{-4}	0.7912	3.610×10^{-3}	1.401×10^{-2}	1.080×10^{-2}		
7	2.4012	10.58	26.86	618.7	180.1	2.426	0.7080	3.816×10^{-4}	0.9756	3.610×10^{-3}	1.432×10^{-3}	1.080		
9	2.4890	1411	71.70	2.479×10^{4}	130.5	12.58	0.7080	3.839×10^{-4}	0.9756	3.610×10^{-3}	1.432×10^{-3}	1.080×10^{-2}	9.785×10^{-6}	1.664×10^{-12}
10	2.5316	5008	108.0	5.587×10^{4}	271.4	28.86	0.7057	1.358×10^{-4}	0.9756	2.408×10^{-3}	1.440×10^{-2}	1.077×10^{-2}	1.816×10^{-2}	3.105×10^{-4}
11	2.7579	1781	116.6	2.279×10^{4}	136.1	16.98	0.7057	1.358×10^{-4}	0.9756	0.1216	1.441×10^{-2}	6.360×10^{-2}	1.790×10^{-2}	1.739×10^{-2}
12	2.9920	1383	124.2	1.837×10^{4}	188.6	11.09	0.7057	1.401×10^{-4}	0.9756	0.1774	1.441×10^{-2}	0.2911	1.795×10^{-2}	2.190×10^{-2}
13	3.2633	3661	157.9	4.141×10^{4}	217.0	16.89	0.7057	1.487×10^{-4}	0.9756	7.737×10^{-2}	1.448×10^{-2}	0.9454	1.832×10^{-2}	2.248×10^{-2}

* 10^8 yr

† 10^{17} dynes/cm^2

‡ 10^6 °K

§ gm/cm^3

‖ 3.86×10^{33} erg/sec

\# 6.96×10^{10} cm

REFERENCES

Caughlan, G. R. and Fowler, W. A. 1964, Ap. J., 139, 1180.

Clayton, D. D. 1964, private communication.

Fowler, W. A. and Hoyle, F. 1964, Ap. J. Suppl. No. 91, 201.

Haselgrove, C. B. and Hoyle, F. 1956, M.N., 116, 515.

Hofmeister, R., Kippenhahn, R. and Weigert, A. 1964, Zs. f. Ap., 60, 57.

Iben, I. Jr. 1964, Ap. J., 140, 1631.

_____ 1965, Ap. J., 000, 000.

Wallerstein, G. 1965, private communication.

FIGURE CAPTIONS

Fig. 1. Path in the theoretical Hertzsprung-Russell diagram for a 3 $M_\odot$ population I star. Luminosity L is in units of 3.86×10^{33} erg/sec and surface temperature T_e is in units of ^oK.

Fig. 2. The variation with time (units of 10^8 yr) of luminosity (L), surface temperature (T_e), mass fraction in the convective core (M_{cc}), and central abundance by mass of $H^1(X_H)$, $He^4(X_4)$, $C^{12}(X_{12})$, $O^{16}(X_{16})$, and $O^{18}(X_{18})$. The unit of luminosity is $L_\odot = 3.86 \times 10^{33}$ erg/sec and the unit of surface temperature is ^oK. Vertical scale limits correspond to $1.95 \leq \log (L) \leq 2.45$, $3.3 \leq \log (T_e) \leq 4.3$, $0 \leq M_{cc} \leq 1/3$. To the left of the break in t, $0.0 \leq X_{16} \leq 0.02$, $0.0 \leq X_H, X_4 \leq 1.0$. To the right of the break in t, $0.0 \leq X_{18} \leq 0.1$ and $0.0 \leq X_4, X_{12}, X_{16} \leq 1.0$.

Fig. 3. The variation with time (units of 10^8 yr) of radius (R), central density (ρ_c), central temperature (T_c), and the rate of energy production by helium burning relative to the rate of energy production by hydrogen burning (L_{He}/L_H). Units are $R_\odot = 6.96 \times 10^{10}$ cm for radius, 10^6 ^oK for temperature, and gm/cm^3 for density. To the left of the break in t, scale limits correspond to $0 \leq R \leq 5$, $21 \leq T_c \leq 31$, and $30 \leq \rho_c \leq 80$. To the right of the break in t, scale limits correspond to $0 \leq R \leq 50$, $1.3 \leq \log (T_c) \leq 2.3$, and $0.5 \leq \log (\rho_c) \leq 5.5$. The ratio L_{He}/L_H is allowed to vary from 0 to 1.

Fig. 4. The variation with mass fraction of state and composition variables when $t = 2.4586 \times 10^6$ yr. Variables have the significance: P = pressure, T = temperature, ρ = density, L = luminosity, R = radius, X_i = abundance by mass of He^3 (X_3), C^{12} (X_{12}), and N^{14} (X_{14}). The maximum value of

each variable in the interior is set equal to unity. Maximum values in physical units are listed in Table 2.

Fig. 5. The distribution versus mass fraction of state and composition variables when $t = 1.9924 \times 10^8$ yr. Variables have the same significance as in Figure 4. In addition are shown the abundances by mass of H^1 (X_H) and O^{16} (X_{16}). Maximum values are given in Table 2.

Fig. 6. The variation with time (10^8 yr) of central density (ρ_c), central temperature (T_c), luminosity (L), mass fraction in the convective core (M_{cc}), mass fraction outside of which energy is transported by convection (M_{CE}), mass fraction inside of which 90 per cent of the total nuclear energy production occurs (M_{90}), and mass fraction outside of which 90 per cent of the total nuclear energy production occurs (M_{10}). Units and vertical scale values for log (L), log (ρ_c), log (T_c), and M_{cc} are the same as in Figure 2. Units and scale values for L_n are the same as those for L. Finally $0 \leq M_{10}, M_{90}, M_{CE} \leq 1$.

Fig. 7. The variation with mass fraction of state and composition variables when $t = 2.4012 \times 10^3$ yr. Variables have the same significance as in Figures 4 and 5. Maximum values of the variables are in Table 2.

Fig. 8. The variation with mass fraction of state variables in the vicinity of the shell source for times $t_1 = 2.4786 \times 10^8$ yr and $t_2 = 2.4869 \times 10^8$ yr. Scale limits correspond to $0 \leq$ density ρ (gm/cm^3) ≤ 250, $7.5 \leq$ temperature T (10^6 ^oK) ≤ 32.5, $0 \leq$ luminosity L (3.86×10^{33} erg/sec) ≤ 250, $0 \leq$ the abundance of hydrogen by mass $X_H \leq 1.0$, and $0 \leq$ radius R (6.96×10^{10} cm) ≤ 0.25. Scale limits for matter velocity v are -10^{-4} cm/sec and $+1.5 \times 10^{-4}$ cm/sec.

Fig. 9. The variation with mass fraction of state and composition variables when $t = 2.4890 \times 10^8$ yr. Variables have the same significance as in Figures 4 and 5. Maximum values of the variables are given in Table 2.

Fig. 10. The variation with mass fraction of state and composition variables when $t = 2.5316 \times 10^8$ yr. Variables have the same significance as in Figures 4 and 5. Maximum values of the variables are given in Table 2.

Fig. 11. The variation with mass fraction of state and composition variables when $t = 2.7579 \times 10^8$ yr. Variables have the same significance as in Figures 4 and 5. Maximum values of the variables are given in Table 2.

Fig. 12. The variation with mass fraction of state and composition variables when $t = 2.9920 \times 10^8$ yr. Variables have the same significance as in Figures 4 and 5. Maximum values of the variables are given in Table 2.

Fig. 13. The variation with mass fraction of state and composition variables when $t = 3.2633 \times 10^8$ yr. Variables have the same significance as in Figures 4 and 5. Maximum values of the variables are given in Table 2.

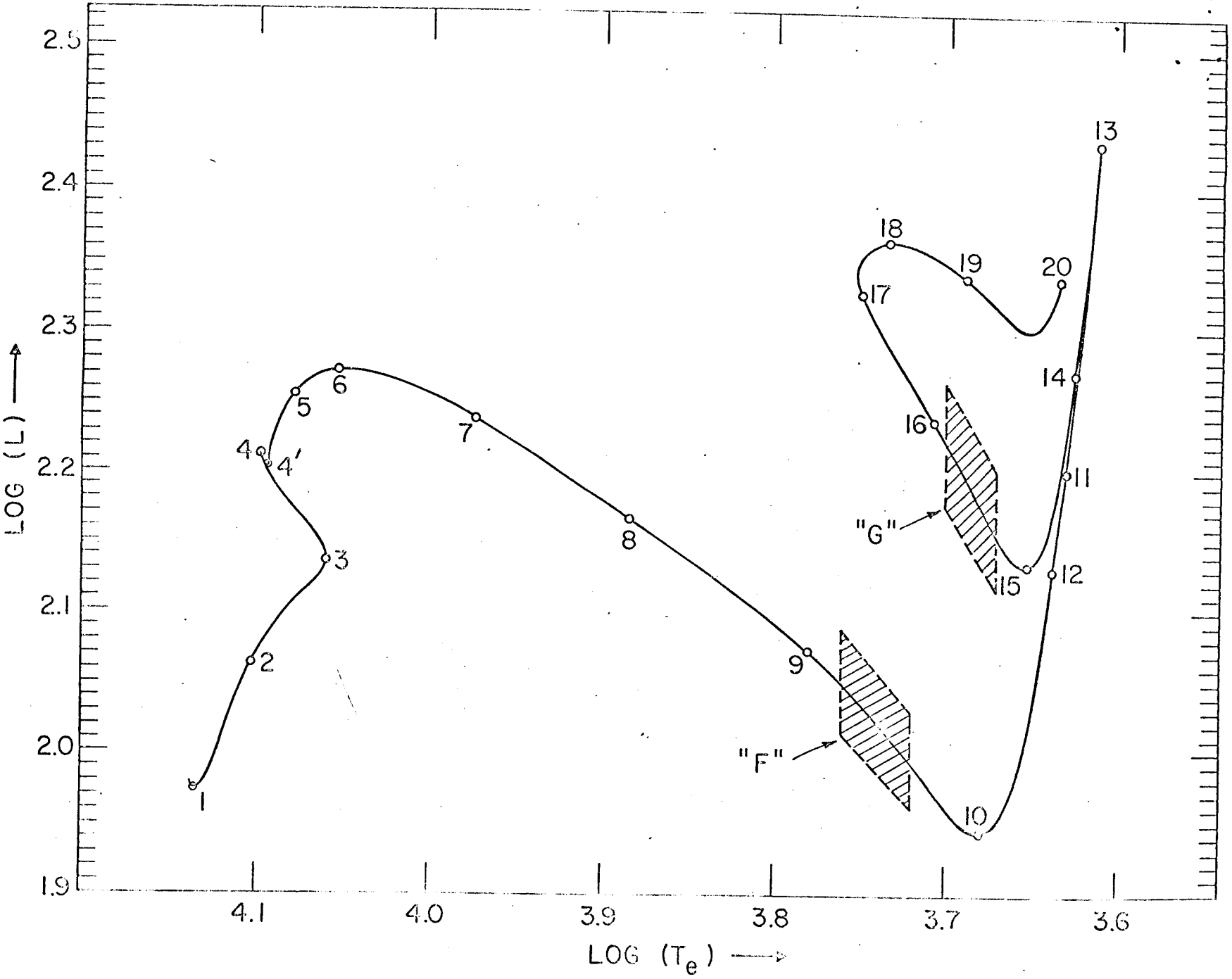
2.5
2.4
2.3
2.2
2.1
2.0
1.9
LOG (L) ⟶
4.1
4.0
3.9
3.8
3.7
3.6
LOG (T_e) ⟶
1
2
3
4
4'
5
6
7
8
9
10
11
12
13
14
15
16
17
18
19
20
"F"
"G"

Fig. 1

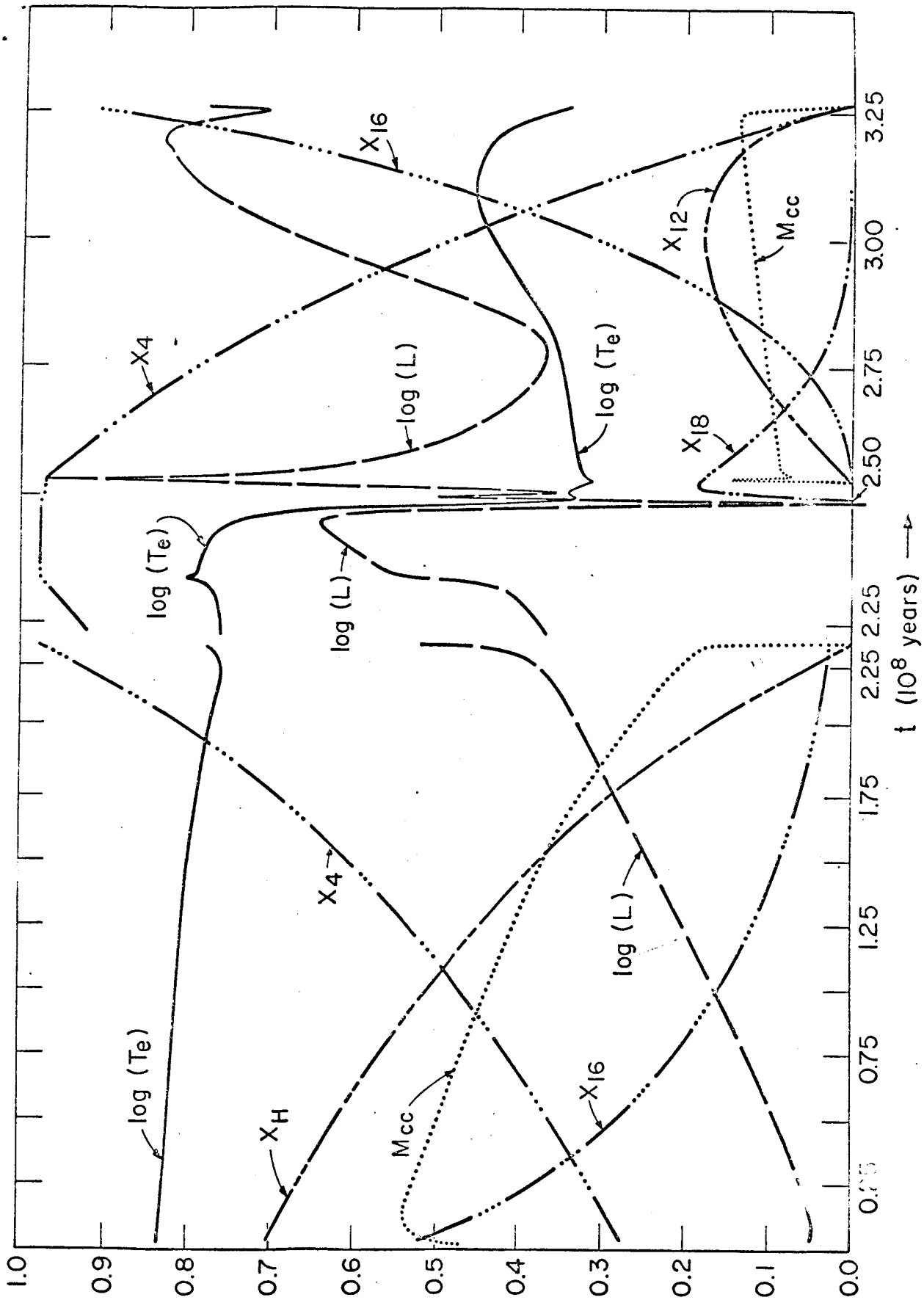
1.0
0.9
0.8
0.7
0.6
0.5
0.4
0.3
0.2
0.1
0.0
0.75
1.25
1.75
2.25
2.25
2.50
2.75
3.00
3.25
t (10^8 years) →
X_H
X_4
X_{16}
M_{cc}
log (L)
log (T_e)
X_{12}
X_{18}

Fig. 2

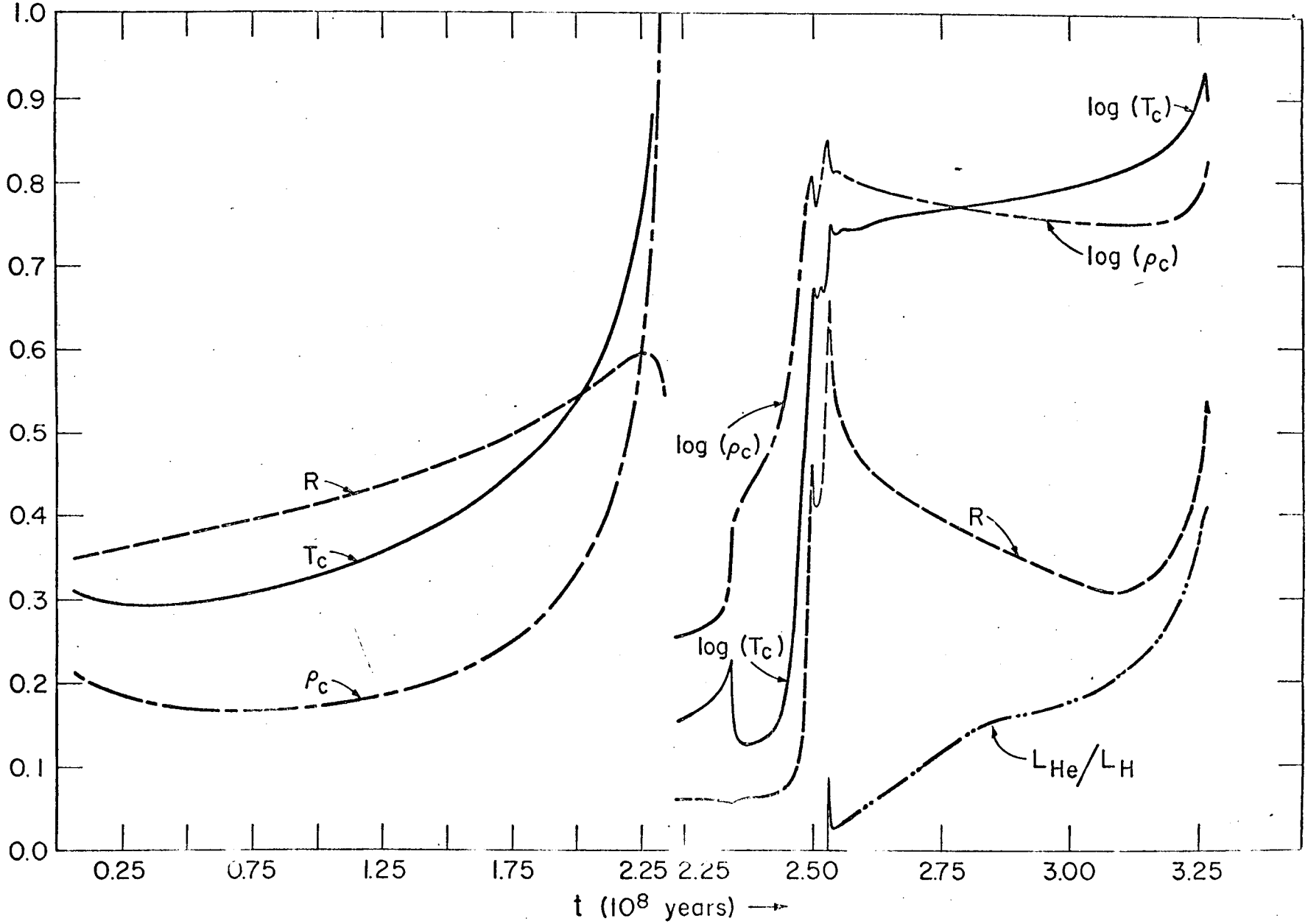
1.0
0.9
0.8
0.7
0.6
0.5
0.4
0.3
0.2
0.1
0.0
0.25
0.75
1.25
1.75
2.25
2.25
2.50
2.75
3.00
3.25
t (10^8 years) →
R
Tc
ρc
log (Tc)
log (ρc)
log (ρc)
R
log (Tc)
LHe/LH

Fig. 3

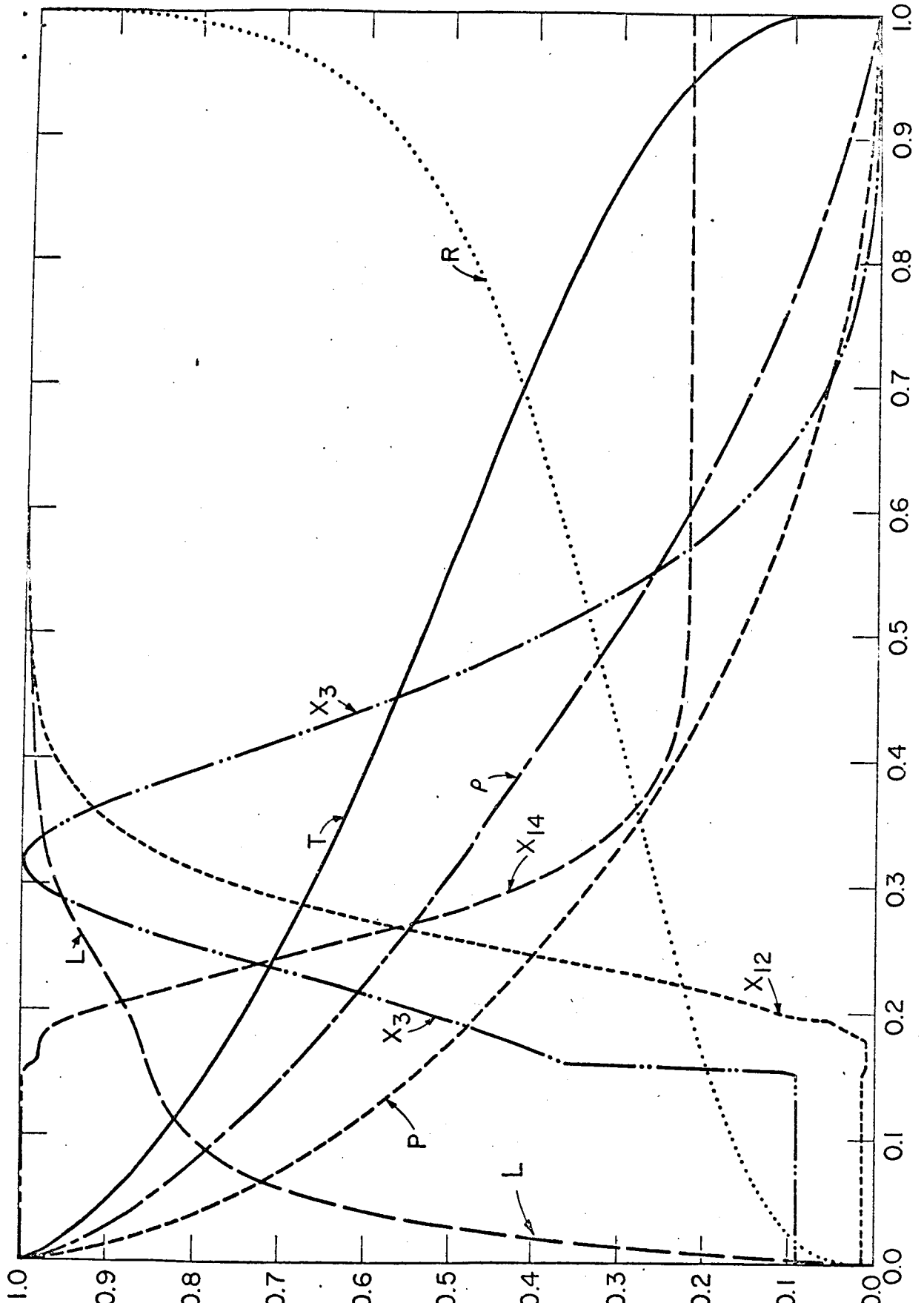
R
T
P
X14
X12
X3
X3
L
P
L
MASS FRACTION
0.0
0.1
0.2
0.3
0.4
0.5
0.6
0.7
0.8
0.9
1.0

Fig. 4

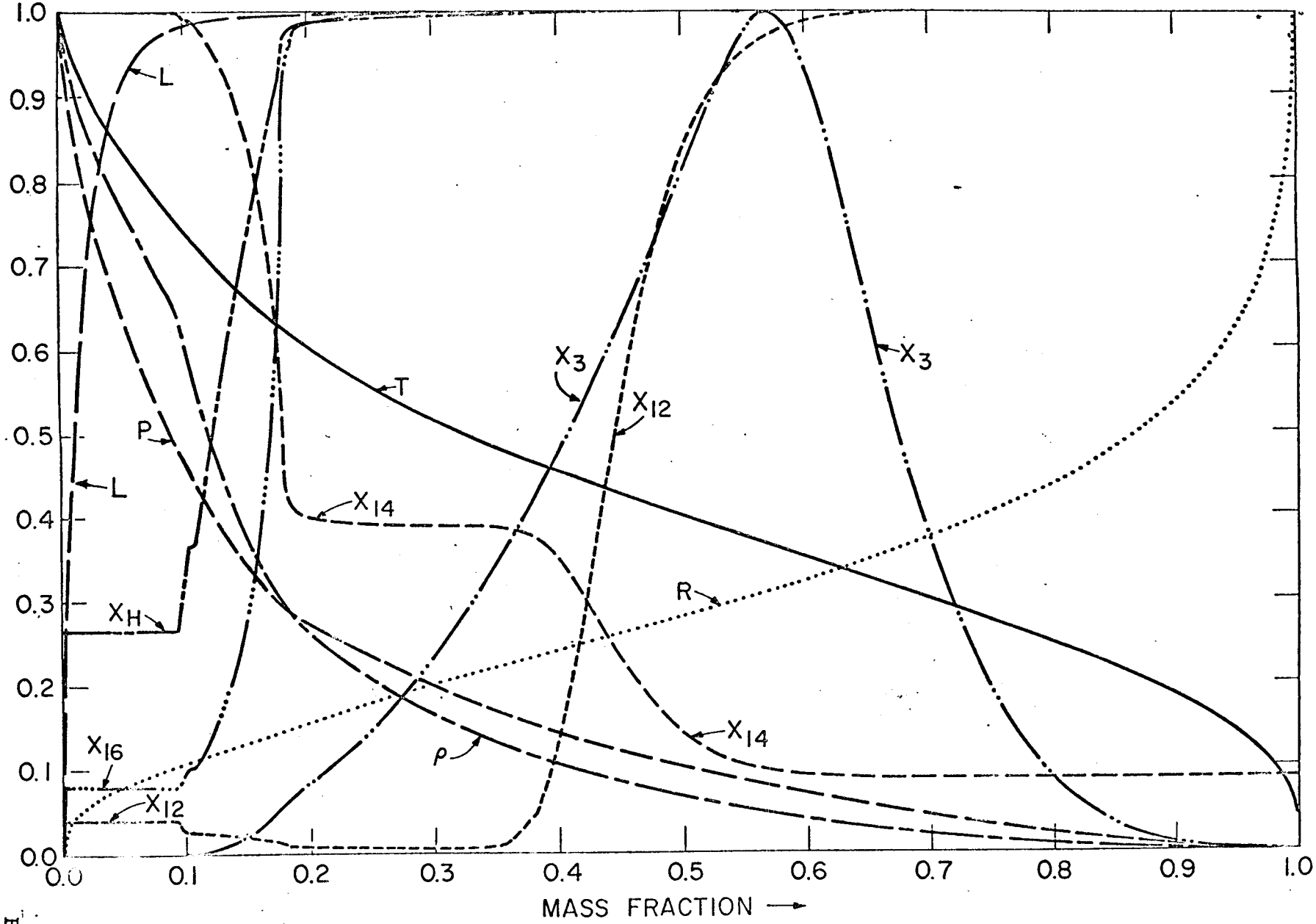
1.0
0.9
0.8
0.7
0.6
0.5
0.4
0.3
0.2
0.1
0.0
0.0
0.1
0.2
0.3
0.4
0.5
0.6
0.7
0.8
0.9
1.0
MASS FRACTION →
L
T
P
L
X_3
X_{12}
X_3
X_{14}
R
X_H
X_{14}
X_{16}
ρ
X_{12}

Fig. 5

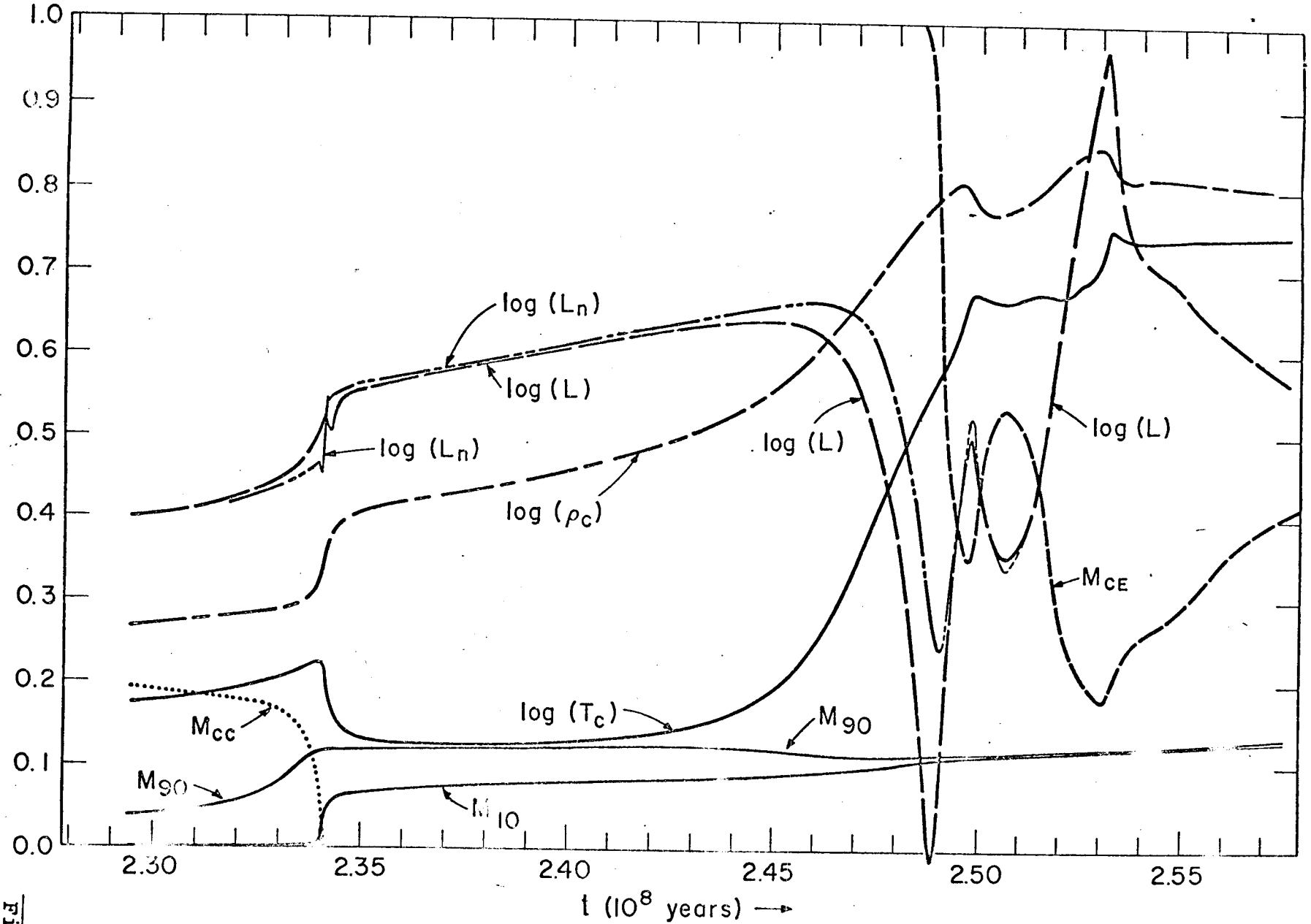
1.0
0.9
0.8
0.7
0.6
0.5
0.4
0.3
0.2
0.1
0.0
2.30
2.35
2.40
2.45
2.50
2.55
t (10^8 years) →
log (L_n)
log (L)
log (L_n)
log (ρ_c)
log (L)
log (L)
M_{CE}
log (T_c)
M_{cc}
M_{90}
M_{90}
M_{10}

FIG. 6

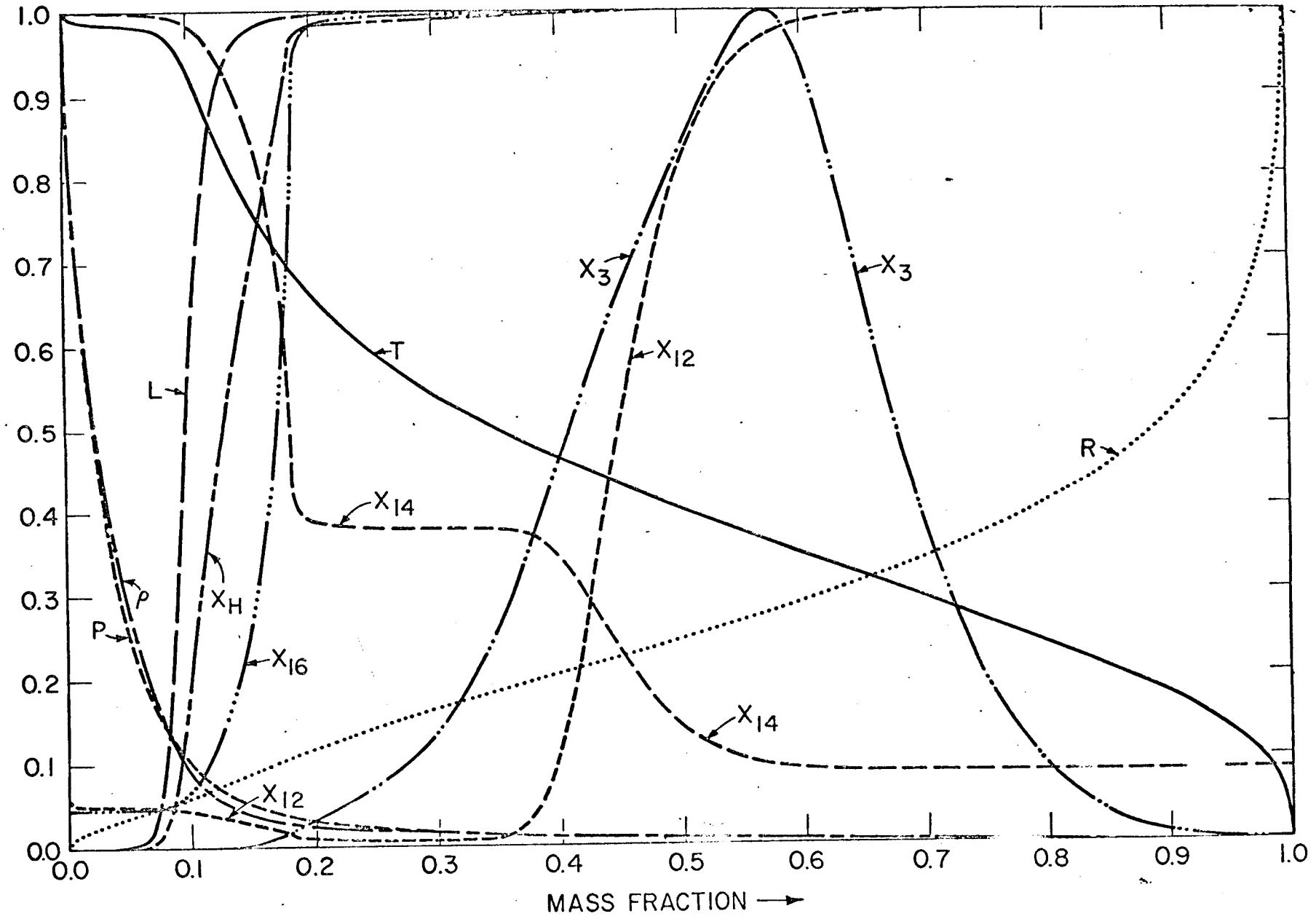
1.0
0.9
0.8
0.7
0.6
0.5
0.4
0.3
0.2
0.1
0.0
0.0
0.1
0.2
0.3
0.4
0.5
0.6
0.7
0.8
0.9
1.0
MASS FRACTION
L
T
R
P
ρ
X_H
X_3
X_3
X_{12}
X_{14}
X_{16}
X_{14}
X_{12}

FIG. 7

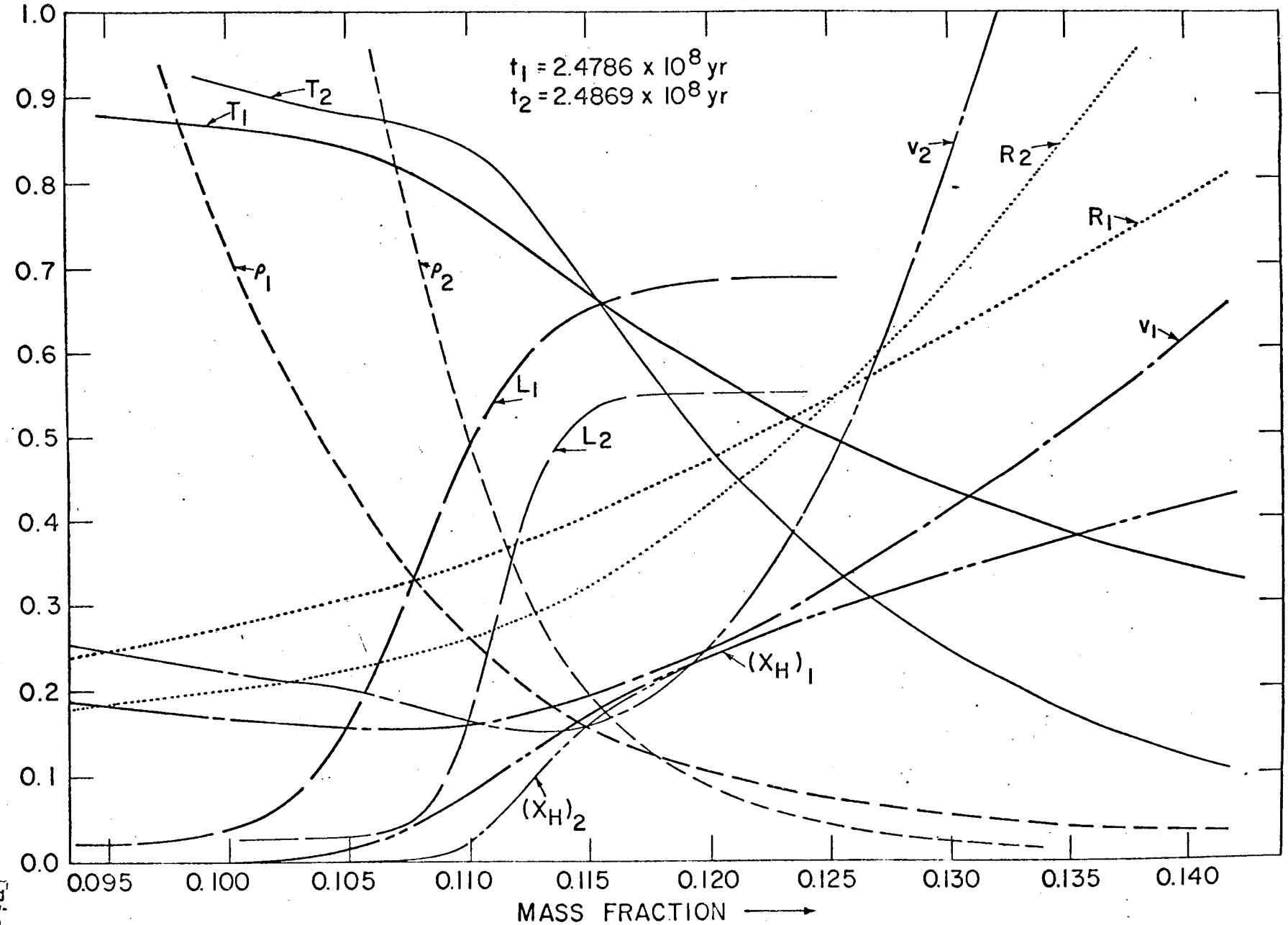
$t_1 = 2.4786 \times 10^8$ yr
$t_2 = 2.4869 \times 10^8$ yr
T_1
T_2
ρ_1
ρ_2
L_1
L_2
v_1
v_2
R_1
R_2
$(X_H)_1$
$(X_H)_2$
1.0
0.9
0.8
0.7
0.6
0.5
0.4
0.3
0.2
0.1
0.0
0.095
0.100
0.105
0.110
0.115
0.120
0.125
0.130
0.135
0.140
MASS FRACTION

Fig. 8

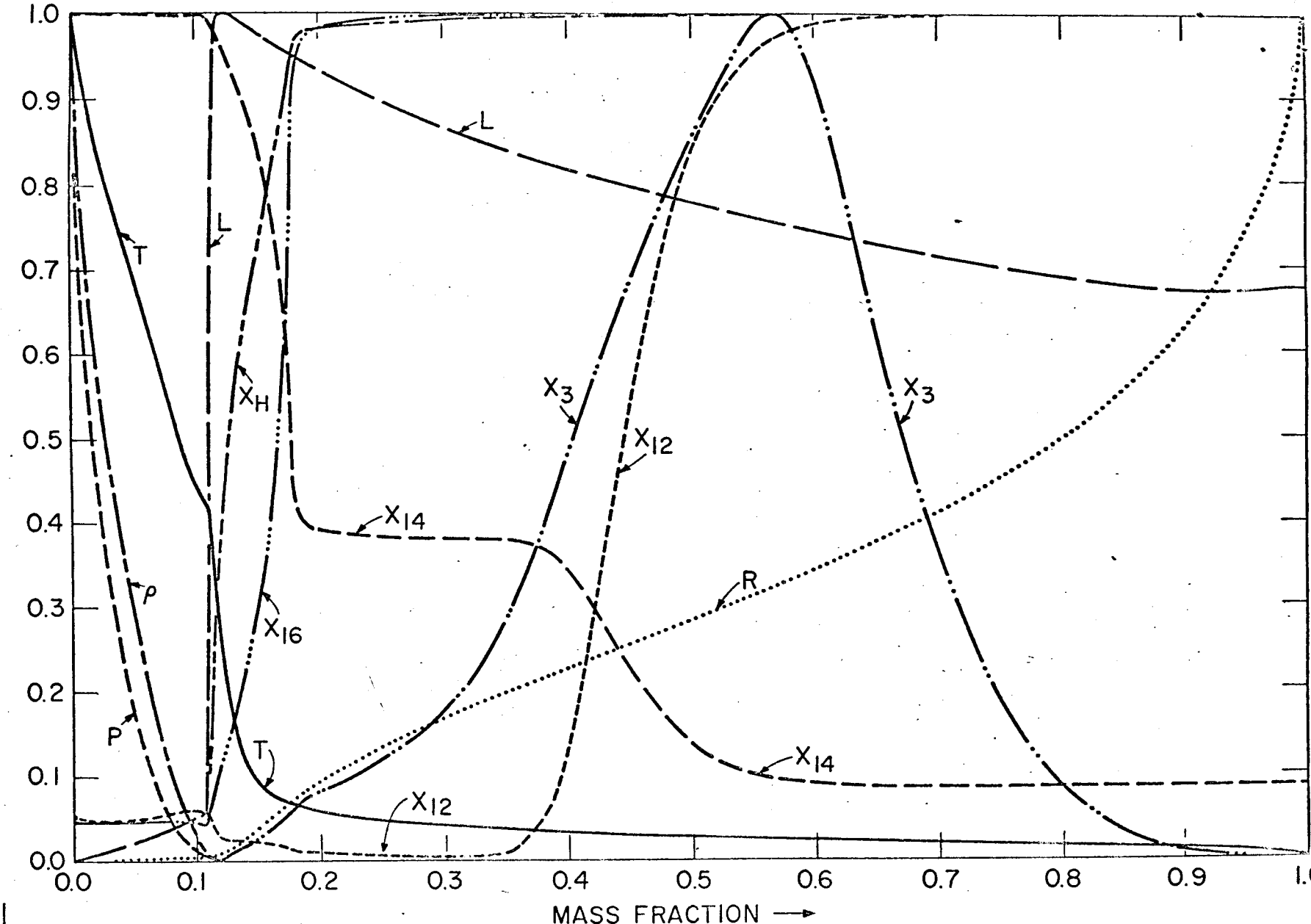
1.0
0.9
0.8
0.7
0.6
0.5
0.4
0.3
0.2
0.1
0.0
0.0
0.1
0.2
0.3
0.4
0.5
0.6
0.7
0.8
0.9
1.0
MASS FRACTION →
L
T
L
X_H
X_3
X_{12}
X_{14}
X_3
ρ
X_{16}
R
P
T
X_{14}
X_{12}

FIG. 9

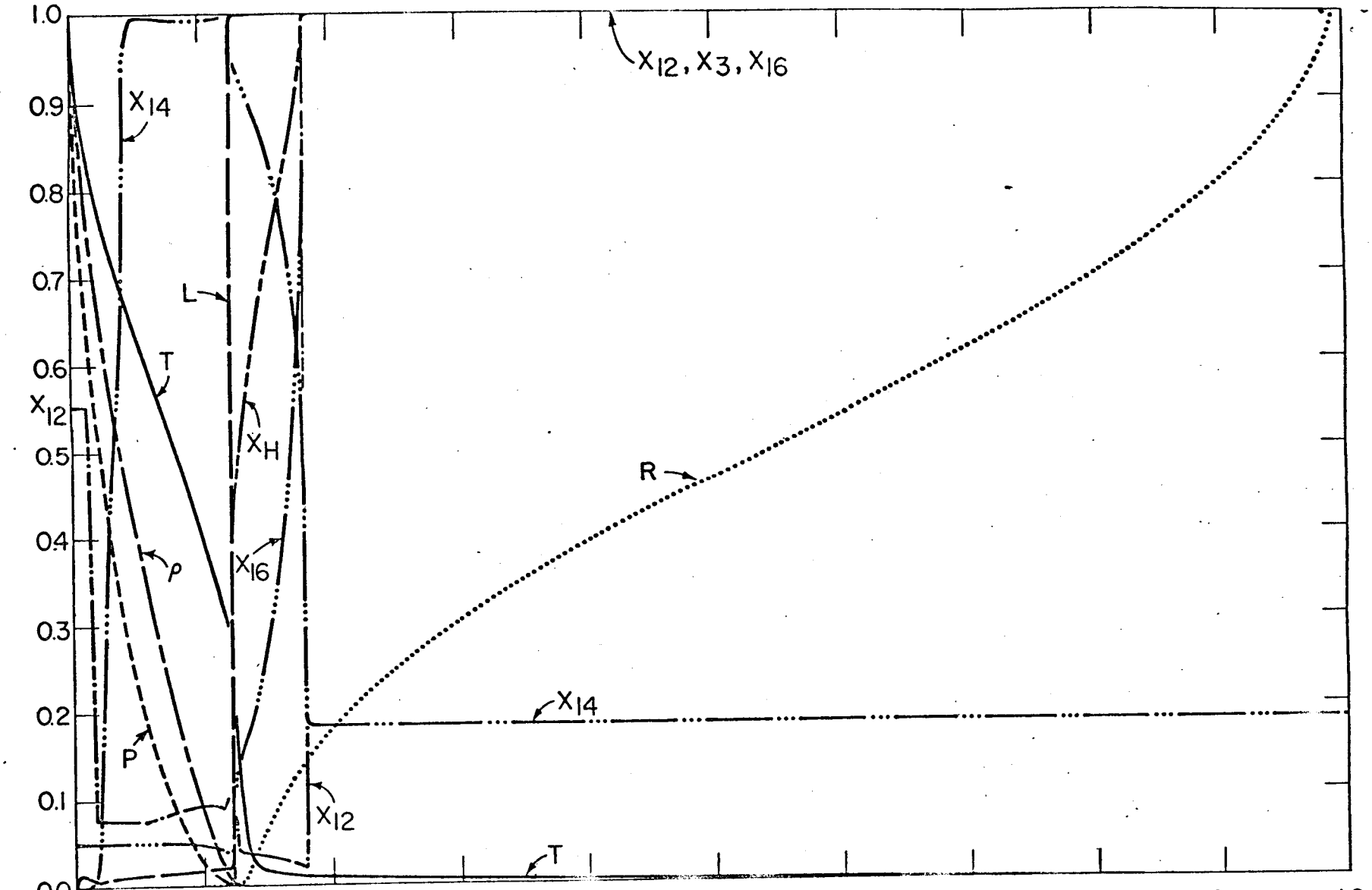
1.0
0.9
0.8
0.7
0.6
0.5
0.4
0.3
0.2
0.1
0.0
X_{12}
X_{14}
L
T
X_H
ρ
X_{16}
P
X_{12}
T
X_{12}, X_3, X_{16}
R
X_{14}
0.0
0.1
0.2
0.3
0.4
0.5
0.6
0.7
0.8
0.9
1.0
MASS FRACTION →

Fig. 10

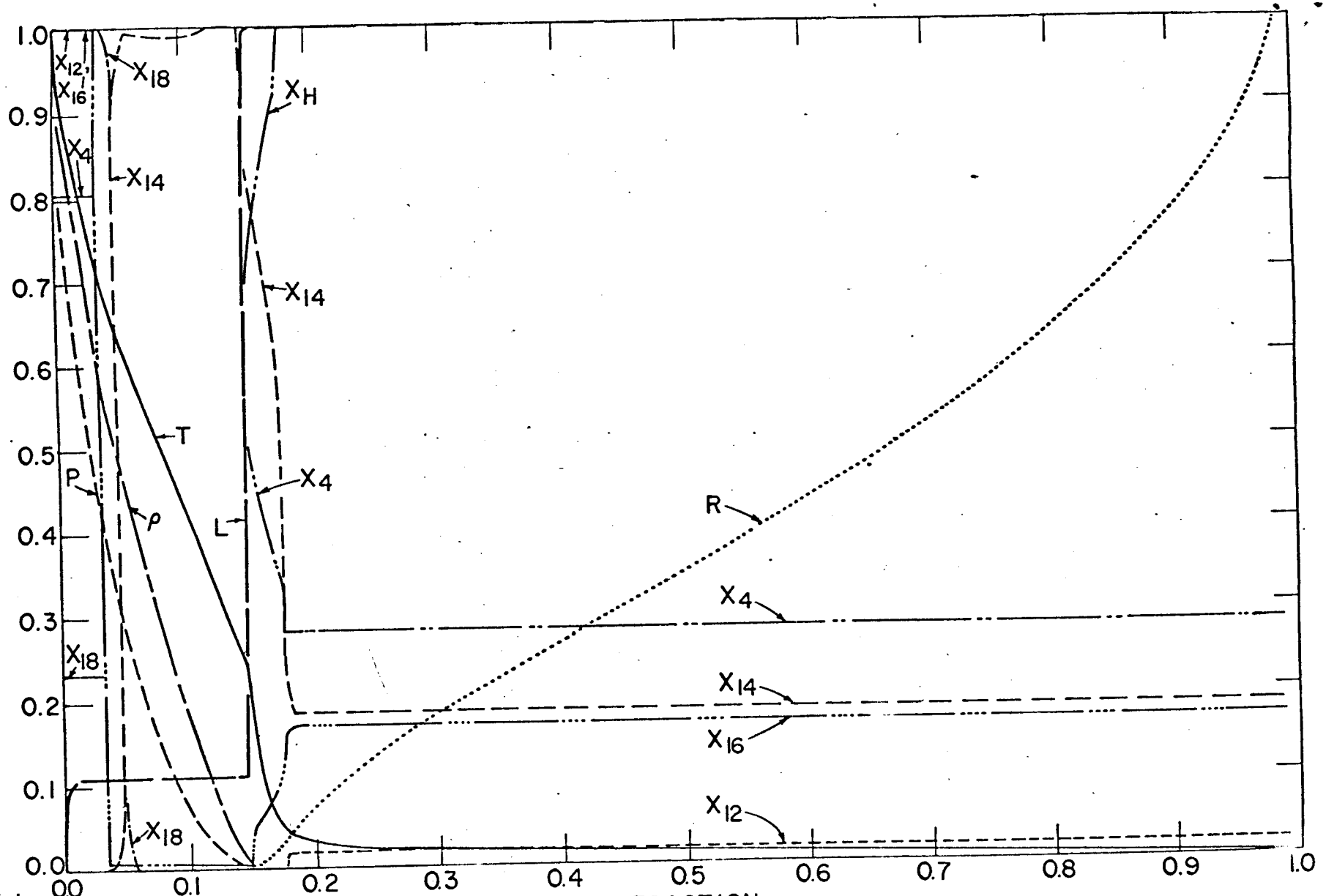
1.0
0.9
0.8
0.7
0.6
0.5
0.4
0.3
0.2
0.1
0.0
0.0
0.1
0.2
0.3
0.4
0.5
0.6
0.7
0.8
0.9
1.0
MASS FRACTION
X_{12}
X_{16}
X_{18}
X_H
X_4
X_{14}
T
P
ρ
L
R

Fig. 11

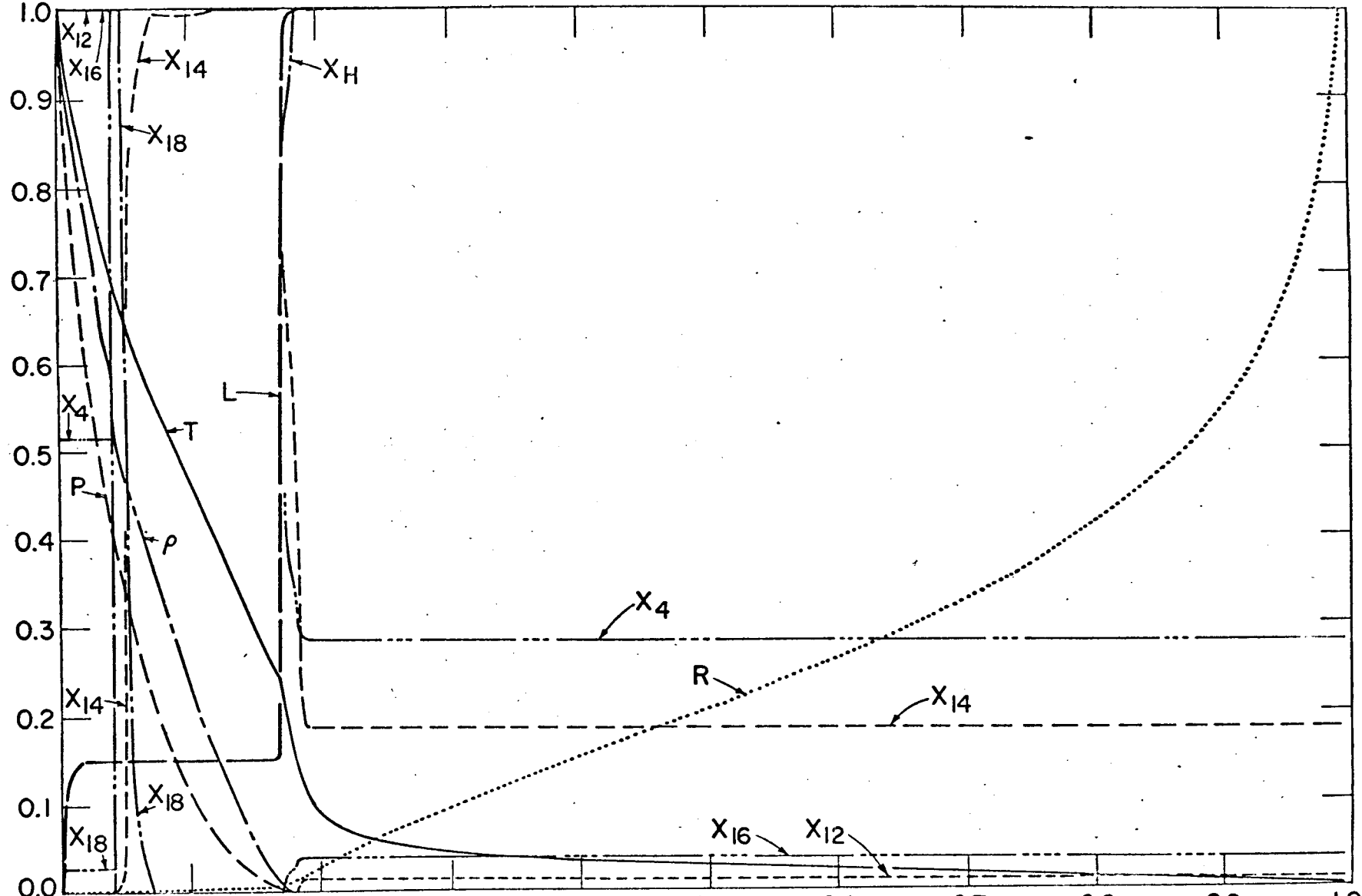
1.0
0.9
0.8
0.7
0.6
0.5
0.4
0.3
0.2
0.1
0.0
0.0
0.1
0.2
0.3
0.4
0.5
0.6
0.7
0.8
0.9
1.0
MASS FRACTION
X_{12}
X_{16}
X_{14}
X_H
X_{18}
L
T
X_4
P
ρ
R

Fig. 12

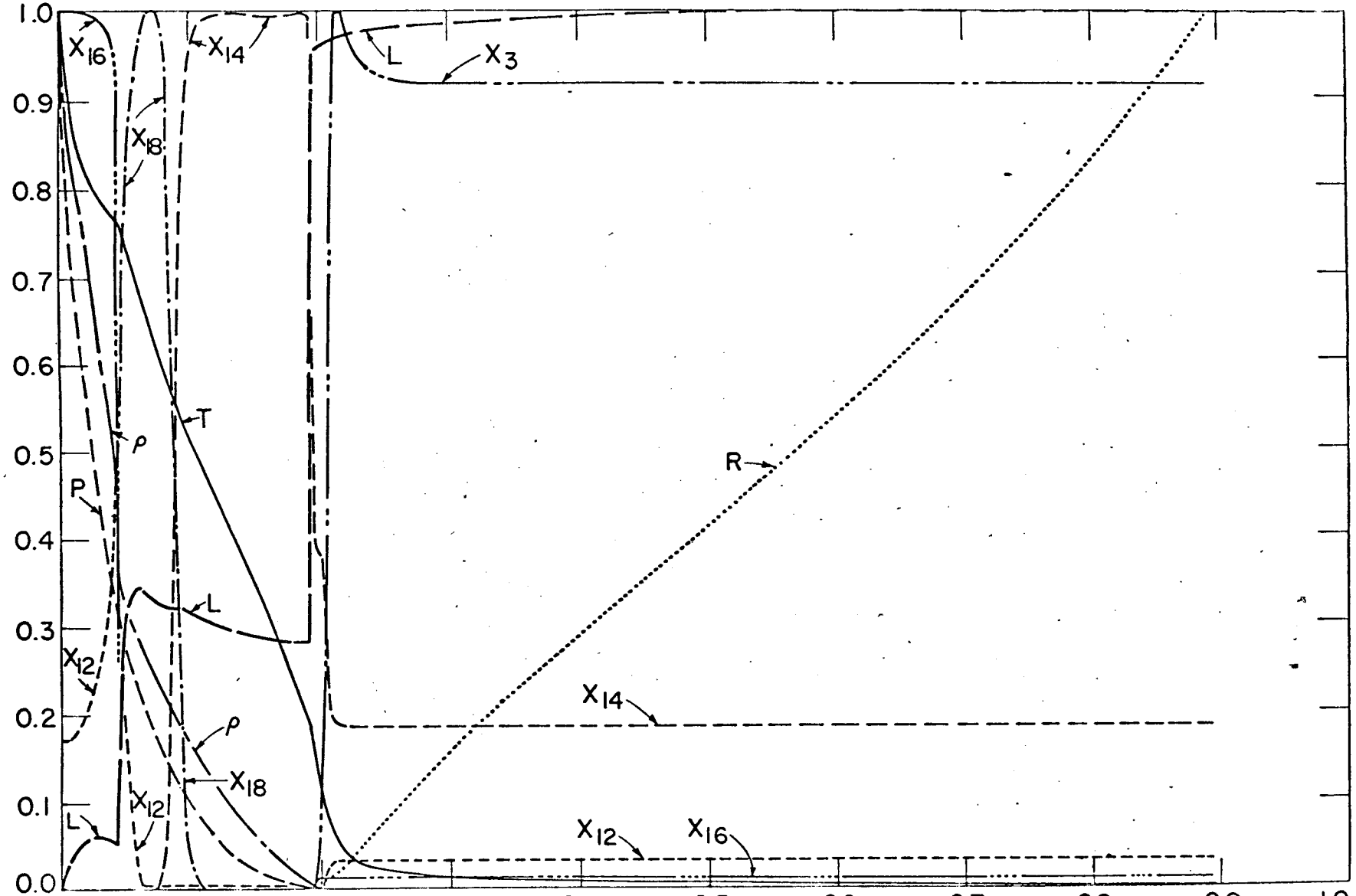
1.0
0.9
0.8
0.7
0.6
0.5
0.4
0.3
0.2
0.1
0.0
0.0
0.1
0.2
0.3
0.4
0.5
0.6
0.7
0.8
0.9
1.0
MASS FRACTION
X16
X14
L
X3
X18
T
ρ
P
R
L
X12
X14
ρ
X18
X12
L
X12
X16

Fig. 13